Polish J. Chem., **78**, 1457–1476 (2004)

Composite Ni-P + TiO_2 Electrocoatings for Hydrogen Evolution Reaction in Alkaline Solutions[*]

by B. Łosiewicz[1], A. Budniok[1], A. Lasia[2] and E. Łągiewka[1]**

[1]*Institute of Materials Science, Silesian University, 40-007 Katowice, Bankowa 12, Poland*
[2]*Département de Chimie, Université de Sherbrooke, Sherbrooke, Québec, J1K 2R1 Canada*

(Received March 3rd, 2004; revised manuscript June 7th, 2004)

Hydrogen evolution reaction (HER) has been studied in alkaline media using three types of electrodes: (*i*) electrocoated with Ni-P + TiO_2, (*ii*) electrocoated with Ni-P + TiO_2 and heated at 400°C, (*iii*) electrocoated with Ni-P + TiO_2 and heated at 500°C. The heating was carried out in argon atmosphere. Topographical and structural changes of Ni-P + TiO_2 coatings before and after heating were investigated applying geometric surface structure (GSS) and X-ray diffraction (XRD) methods. GSS results were presented graphically in 2 and 3 dimensions. Steady-state polarization and *ac* impedance spectroscopy were used to determine electrode activities. HER proceeded *via* Volmer-Heyrovský mechanism. The effectiveness of HER depended on the intrinsic activity. HER was enhanced when heating was applied, due to the increased amount of non-stoichiometric Ti oxides (facilitating H reduction/adsorption), comparing to the unheated Ni-P + TiO_2 electrode. The most efficient HER proceeded under the following conditions: 5 *M* KOH, 25°C, Ni-P + TiO_2 electrode heated to 500°C.

Key words: composite electrocoatings, impedance modeling, hydrogen evolution, porous electrodes, titanium dioxide

Water electrolysis in alkaline media is a non-polluting method of hydrogen production providing high-purity hydrogen. Low-cost production of hydrogen is a key factor for bringing this technology to commercialization [1–6]. Many attempts have been made to optimise the conditions and economic efficiency of hydrogen evolution reaction (HER) in alkaline solutions [1–3,5–7]. The main aim of electrochemical methods of hydrogen production is to reduce the overpotential of HER. For this purpose, one is searching for new electrode materials, which lower the energetic barrier accompanying HER. During the last few decades a great step forward has been made in this field.

Composite nickel-based electrocoatings are used as large-surface electrodes for water electrolysis. They provide an increased surface area and/or an increased intrinsic activity which both decrease overpotential of HER [2,3,5–18]. Our earlier research was focused on Ni-P + TiO_2 coatings obtained by electrodeposition [7,10,12–14]. Their

---

[*] Dedicated to Prof. Dr. Z. Galus on the occasion of his 70th birthday.
[**] Corresponding author. Tel. +48-32-3591582; Fax: +48-32-2596929; e-mail: budniok@us.edu.pl

thickness was equal to the diameter of TiO_2 particles (below 100 μm). They were especially applicable to HER in alkaline solutions. The recent AES studies have revealed that non-stoichiometric Ti_2O_3 is formed at the TiO_2 grains – nickel matrix interface during electrodeposition [7,10,13]. It has been proved that an increase in electrochemical activity of these electrodes is due to the increase in the real surface area, as well as to the presence of both TiO_2 and Ti_2O_3. Their presence at the electrode surface facilitates H reduction/adsorption compared to Ni-P electrodes. Moreover, modification of Ni-P + TiO_2 coatings with metallic Ti powder was performed and Ni-P + TiO_2 + Ti deposits were obtained. These coatings comprised an amorphous Ni-P matrix with the embedded crystalline TiO_2 and Ti particles [7,11,16]. On the surface of these coatings non-stoichiometric $Ti_{10}O_{19}$ and intermetallic NiTi compounds were additionally present. These species were formed at the interface of TiO_2 and Ti grains, and the nickel matrix. The heating of such coatings in the argon atmosphere led to the crystallization of Ni-P matrix and formation of non-stoichiometric titanium oxides ($Ti_{10}O_{19}$, Ti_7O_{13}, Ti_4O_7), which are detectable by XRD method. It has been found that the coatings consisting of Ni-P and mixed titanium oxides exhibited better properties towards HER than Ni-P + TiO_2 coatings, which arose from the unique combination of individual components, as well as from their interactions at particular interfaces [7,11,16]. Moreover, the heating of Ni-P + TiO_2 coatings in argon atmosphere could cause the formation of non-stoichiometric titanium oxides, which enhanced HER kinetics.

In this paper, morphological and structural changes in Ni-P + TiO_2 coatings before and after heating them at various temperatures were investigated applying 2- (2D) and 3- (3D) dimensional GSS methods and X-ray diffraction (XRD). The effect of the heating on the mechanism of HER was studied applying *ac* impedance and steady-state polarization in 5 *M* KOH at 25°C. Kinetic parameters and rate constants were obtained from the experimental results.

EXPERIMENTAL

Electroactive Ni-P + TiO_2 coatings were prepared by electrodeposition of TiO_2 powder (anatase, LOBA FEINCHEMIE, Lot. Nr 17508, 100 mesh) with amorphous nickel-phosphorus on the steel support (St3S). Bath composition and the preparation procedure were described in detail in the previous papers [7,10,13,14].

Except from the one, all the walls of the steel plates were coated with an epoxy resin (Distal) to obtain a (geometric) working surface area of 1 cm^2. Deposition was carried out at a constant cathodic current (j = 250 mA cm^{-2}) for 25 min at 25°C. After deposition, the coatings were rinsed with water, acetone and dried. The mass increase of deposits was estimated as the mass difference before and after electroplating [7,11]. Deposits were heated at 400 and 500°C for 10 h under a stream of argon (99.999%).

GSS studies of the obtained coatings were carried out using a Form Talysurf-type profilograph (Tylor Hobson). Examination of the surface topography was undertaken for two reasons. The first purpose was to determine the surface roughness and waviness from the 2D XY profile using R_a, R_p, R_v, R_z, RS, RL_0 and RL_n parameters. Secondly, the surface topography was studied from its 3D XYZ stereometric image [19,20] within the sampling length l and the maximum profile height (R_p + R_v). Local irregularities were measured with an accuracy of 1% and 10%, respectively.

XRD analysis was performed using a Philips diffractometer and applying CuK_α radiation.

A platinum grid counter electrode of a geometric surface area of 1 dm^2 and the external Hg/HgO/5 *M* KOH reference electrode were placed in a Pyrex® glass cell (Radiometer, No 1734) [7,10,11]. The reference electrode was connected to the cell through the bridge filled with 5 *M* KOH, and a Luggin capillary. The system was kept at the room temperature. The equilibrium potential of the hydrogen electrode was measured using a platinized platinum electrode under the same conditions. A value of (–930 mV) was obtained at 25℃. Electrochemical measurements were carried out at 25 °C in 5 *M* KOH solutions prepared form deionized water and containing 10 g dm^{-3} sodium ethylenediaminetetraacetate (EDTA) to avoid deactivation of the electrode [2,21,22]. The solutions were degassed by purging with argon. The same system was used for the steady-state and *ac* impedance measurements. Alternating current impedance measurements were carried out under the potentiostatic control using an Autolab 20 Potentiostat/Galvanostat with Frequency Response Analyser (FRA) and Differential Electrometer Amplifier (Eco Chemie B.V., the Netherlands). Data processing procedure is explained elsewhere [7–11,16,18]. From the steady-state polarisation experiments the Tafel slope, b ($b = dE/d\log j$), the apparent exchange current density, j_0, and overpotential, η_{100} at the current density of 100 mA cm^{-2}, were obtained.

The values of overpotentials were corrected for the uncompensated resistance, the latter determined by electrochemical impedance spectroscopy (EIS) [2,5–11,16,21,22]. Other experimental details were described in the earlier papers [7,10,11,14].

RESULTS AND DISCUSSION

GSS examinations of coatings. The results of GSS studies of the obtained coatings are consistent with our earlier SEM observations (see Ref. 10, Fig. 1 and Ref. 13, Fig. 2). The surface of Ni-P + TiO_2 deposits before (Fig. 1a) and after heating (Fig. 1b,c) exhibit an island-like topography isotropic in any direction parallel to the surface.

Isometric images of Ni-P + TiO_2 coatings before (Fig. 2a) and after heating (Fig. 2b,c) exhibit an apparent decrease of the deposit roughness with the increase of the temperature. The most developed surface of Ni-P + TiO_2 coatings is observed before heating.

The surface roughness profile and profile dimension of the investigated coatings are presented in Fig. 3a–d. These data were used for the experimental determination of 2*D* GSS parameters (Fig. 4), which were presented graphically. It has occurred that arithmetical mean deviation of the roughness profile, R_a, a ten-point height of irregularities, R_z, a maximum profile peak height, R_p, a maximum profile valley depth, R_v, and an average distance between irregularities, *RS*, decrease with the heating temperature. Moreover, all of them reach the highest values in the case of unheated Ni-P + TiO_2 coating (Fig. 4) [19,20]. From the obtained results it follows that on the surface of this coating, the largest irregularities have a shape of conical islands. They are distributed more sparsely than smaller irregularities of the same shape. The calculated parameter ($RL_0 - RL_n$) (RL_0 – the developed profile length, RL_n – the evaluated profile length) are of the order of magnitude of $0.2RL_n$ (Fig. 4). One may conclude that *Ar* parameter depends on the heating temperature (*Ar* parameter determines a relative increase in the surface area of the deposited coating with respect to the geometric surface area of the sample). Its value decreases from 145 to 121% for unheated and

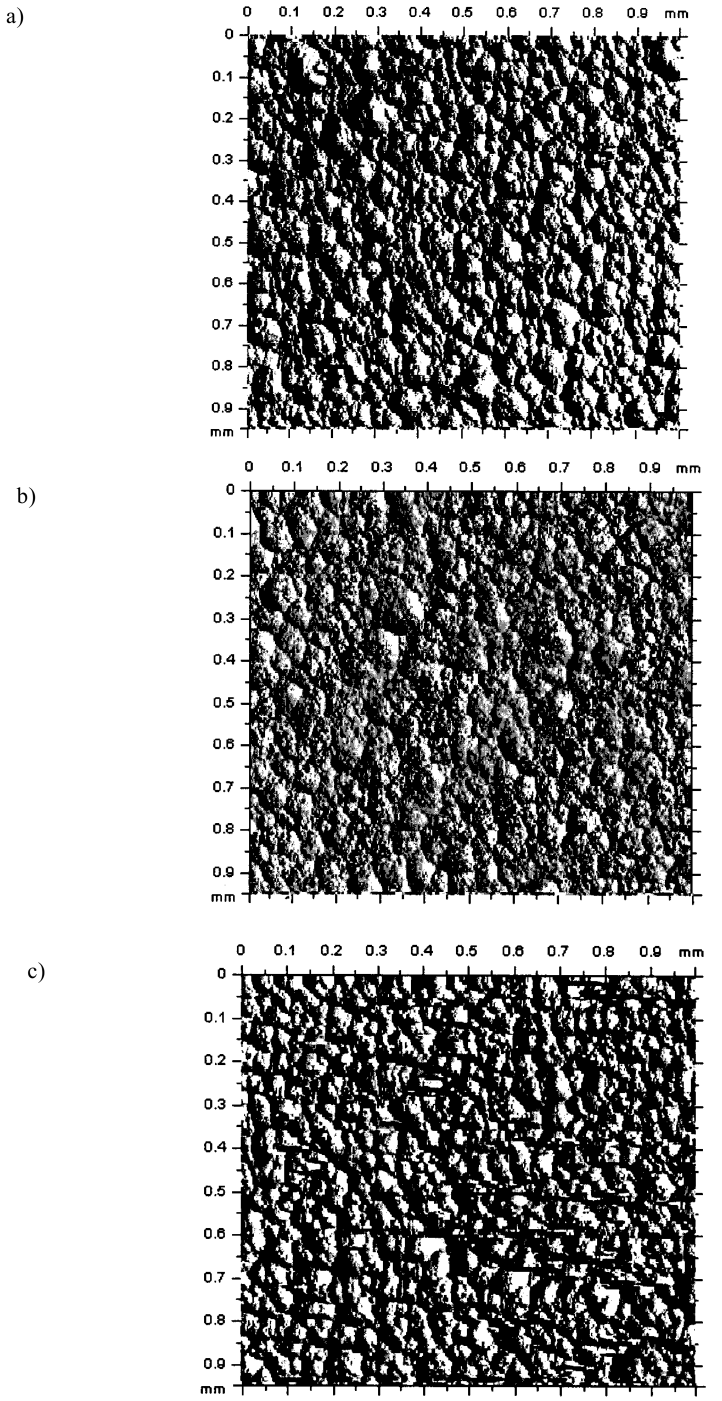

Figure 1. Surface of the Ni-P + TiO_2 coating: as-deposited (a), after heating at 400°C (b) and at 500°C (c) in an argon atmosphere.

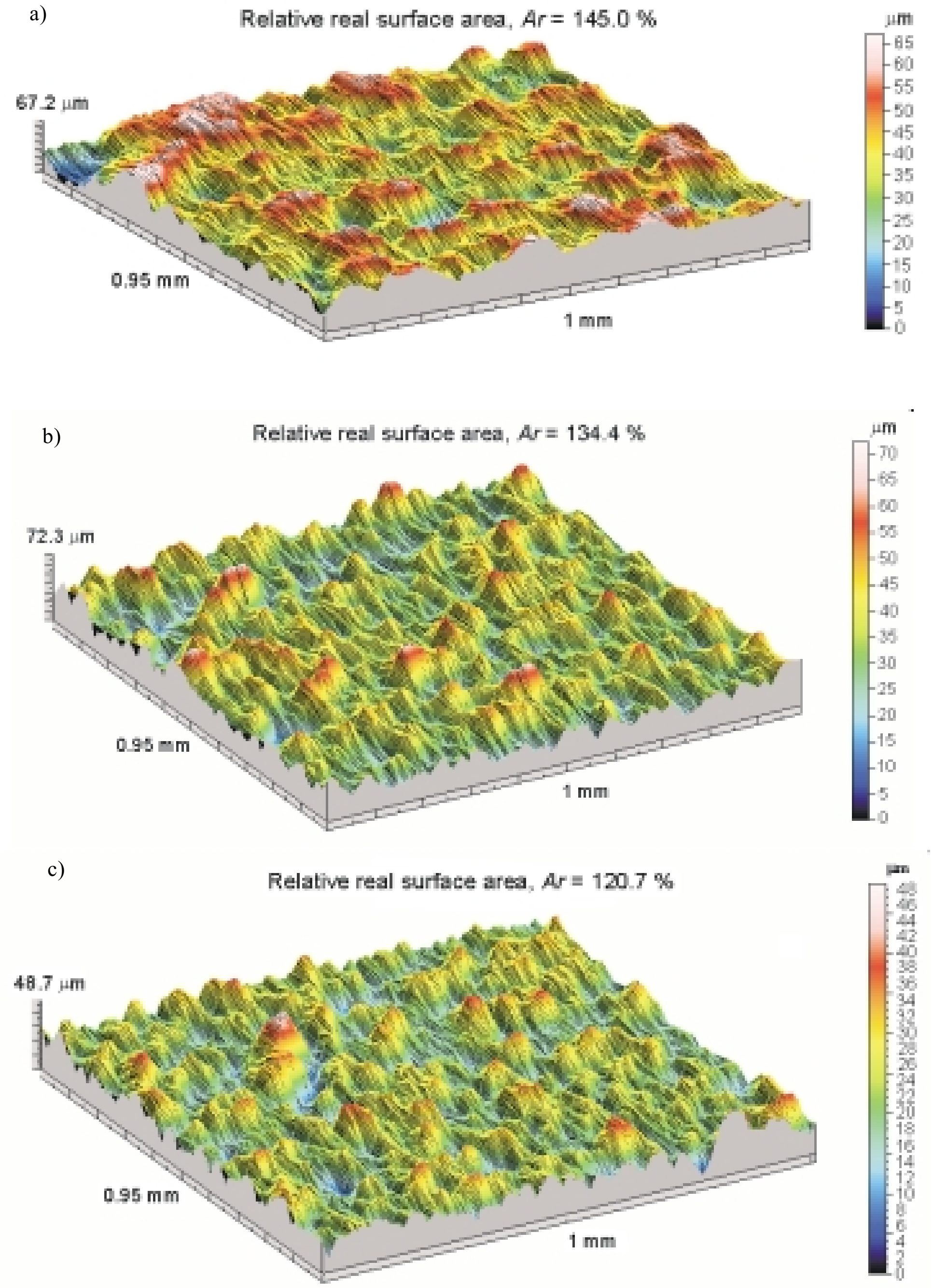
a) Relative real surface area, *Ar* = 145.0 %

b) Relative real surface area, *Ar* = 134.4 %

c) Relative real surface area, *Ar* = 120.7 %

Figure 2. Isometric images of the Ni-P + TiO_2 coating: as-deposited (a), after heating at 400°C (b) and at 500°C (c) in an argon atmosphere.

heated (500°C) Ni-P + TiO_2 coatings, respectively. The *Ar* value of deposits is larger in comparison to the geometric surface area, which is in a good agreement with the results shown in Figs. 1 and 2.

XRD measurements. Figure 5 presents XRD spectra of Ni-P + TiO_2 coatings obtained directly after electrodeposition (Fig. 5a) and after heating at different temperatures (Fig. 5b,c). The XRD spectrum of Ni-P + TiO_2 coating (Fig. 5a) is characteristic for the presence of the amorphous nickel as a matrix in the angular range 2θ comparing to the XRD spectrum of Ni-P deposit obtained under the same conditions [13].

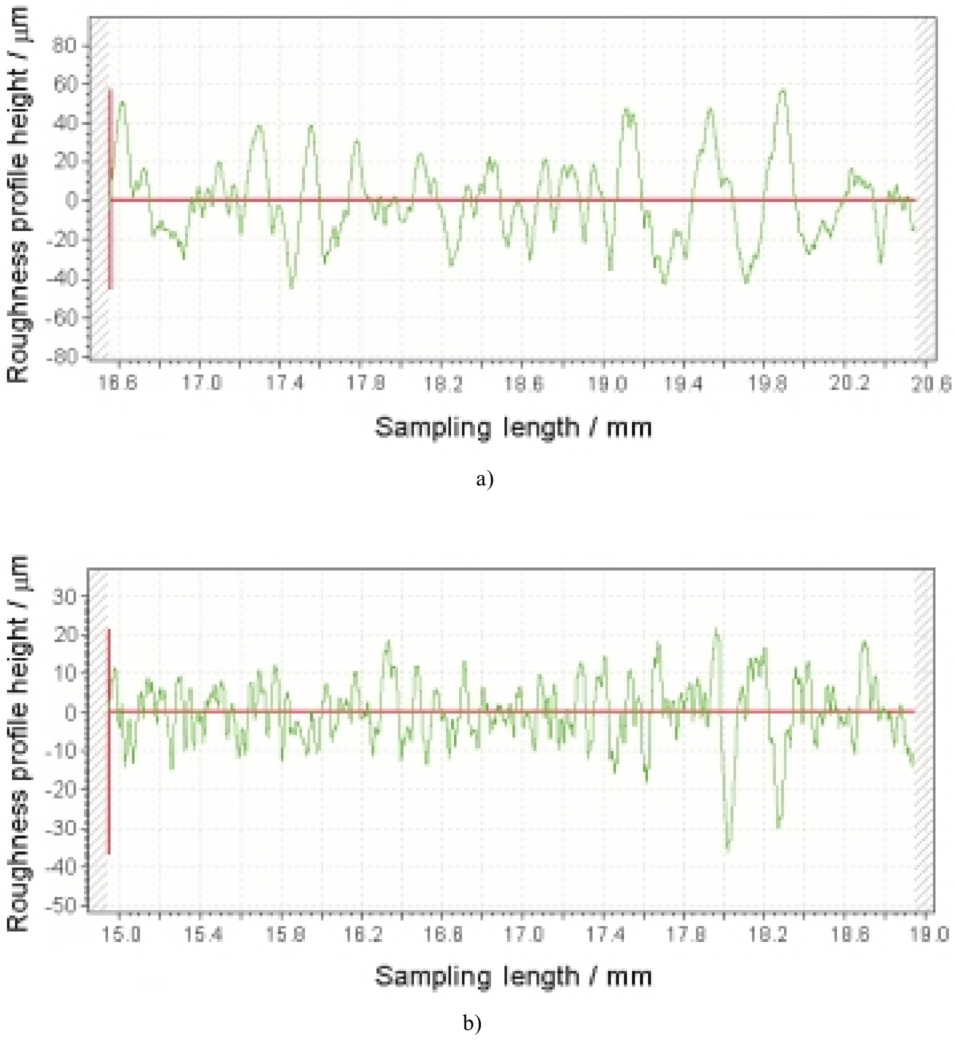

Figure 3. (a) and (b).

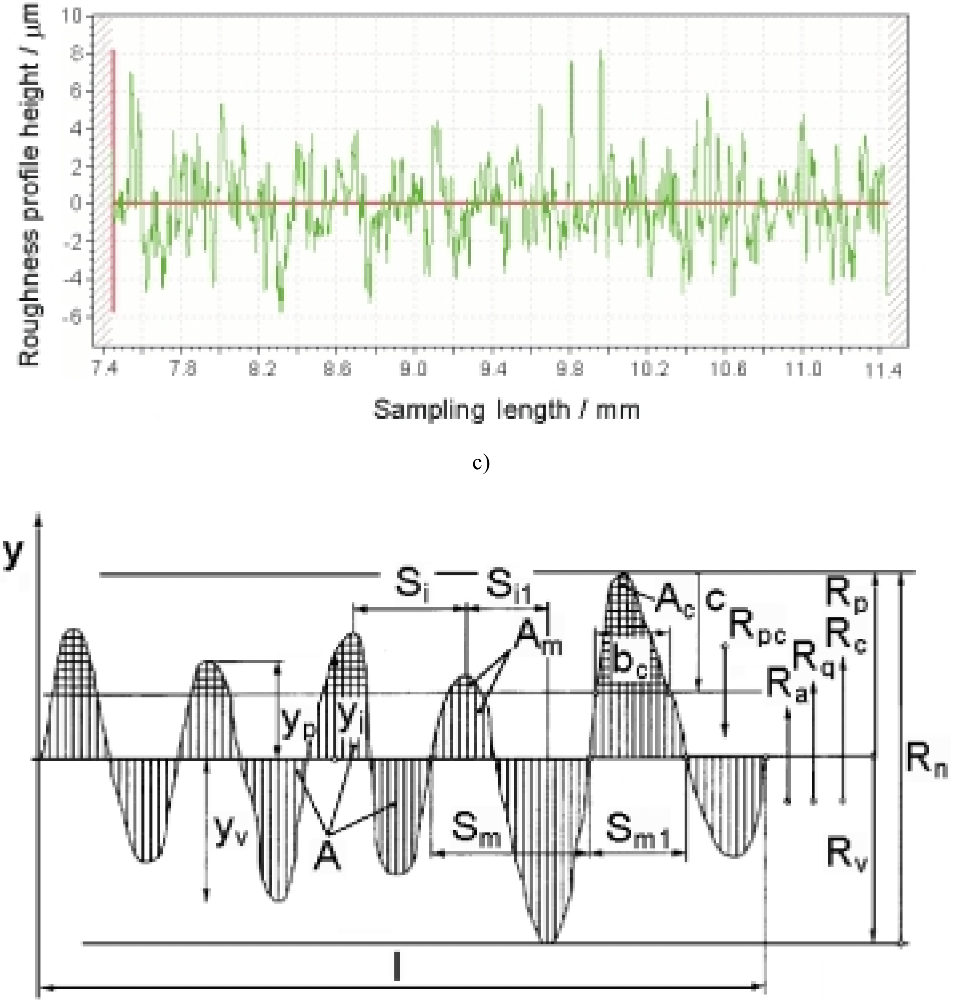

c)

d)

Figure 3. The surface roughness profile of the Ni-P + TiO_2 coating: before (a) and after heating at 400°C (b), and at 500°C (c) in an argon atmosphere, and profile dimension (d).

In Figures 5 b and c XRD spectra of the coatings heated to 400 and 500°C, respectively are shown. The results are in agreement with GSS studies, since both confirm the influence of temperature on the phase composition of Ni-P + TiO_2 coating. In all cases, multiphase systems were formed. After the heating, a broad diffraction band corresponding to the amorphous nickel disappears (Fig. 5a) as a result of the transformation of Ni-P matrix to the system comprising nickel and nickel phosphide (Ni_5P_2) crystallites (Fig. 5b,c). Furthermore, in all XRD spectra of the heated coatings sharp bands (at the same 2θ values) are observed. They originate from the diffraction on a crystalline TiO_2 phase (anatase).

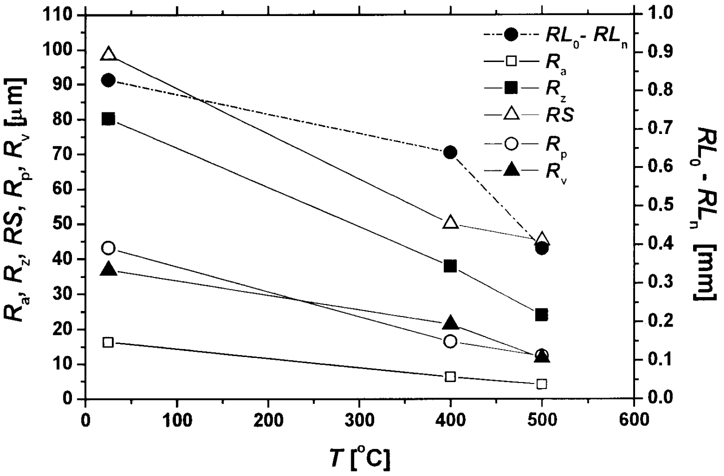

Figure 4. Dependence of 2*D* parameters of geometric surface structure, *GSS*, on heating temperature, *T*, for the surface of Ni-P + TiO_2 coatings. All parameters are defined in text.

In our earlier papers it was postulated that co-deposition of Ni and TiO_2, as well as the reaction of NaH_2PO_2 with Ni^{2+} ions to form Ni_5P_2, may also favour surface reduction of TiO_2 to produce non-stoichiometric titanium oxides, like Ti_2O_3 [7,10,13]. However, after XRD analysis performed before and after heating in argon, any such phase or intermetallic compounds (Ni and Ti) were found. This was probably due to the amorphous structure of these phases or their too small and thus undetectable amounts by XRD technique. The application of AES surface-sensitive method (see Ref. 10, Fig. 3) confirmed the presence of Ti_2O_3 and TiO_2 on the coating surface. This fact may be important for the effectiveness of HER on such electrode support.

Tafel plots. Electrochemical activity of Ni-P + TiO_2 coatings before (A) and after heating them at 400 (B) and 500°C (C) was examined from Tafel plots. Tafel plots for HER in 5 *M* KOH and at 25°C corrected by jR_S are shown in Fig. 6. Corresponding results of the steady-state polarization experiments (b, j_0, η_{100}) are presented in Table 1. All kinetic parameters were determined with respect to the geometric surface areas (1 cm^2) of the coatings. Polarization at the constant current, j = 100 mA cm^{-2}, lasting for two days did not result in any changes of the electrode surfaces detectable either in GSS or XRD.

In the whole potential window in each Tafel curve only one linear range can be distinguished (Fig. 6). For all the coatings, the Tafel slopes are steep (Tab. 1). An increase in the apparent activity was observed after heating the electrode A. As it is seen from Fig. 6 and Table 1, electrodes B and C are characterized by a lower and a higher b value compared to the electrode A, respectively. For electrode B, b = –187 mV dec^{-1}, which is comparable to the b value obtained for the active Ni-P + TiO_2 + Ti electrode after heating it at 400°C in argon [11]. However, the result of GSS studies are inconsistent with those of Brown *et al.* [23,24], who claimed that under the same experimental conditions the Tafel slope is smaller at rough electrodes than at the smooth ones made of the same metal.

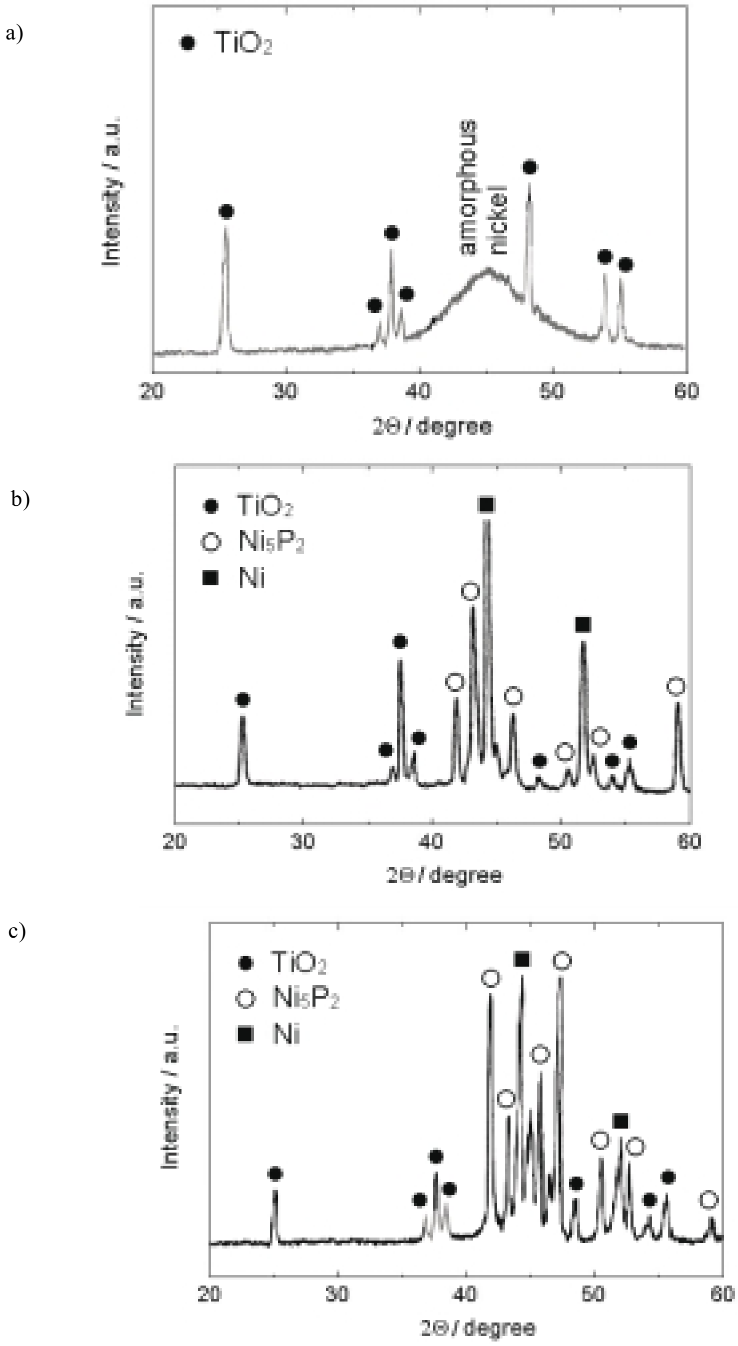

Figure 5. XRD patterns of the Ni-P + TiO_2 coating before (a) and after heating at 400°C (b) and at 500°C (c) in an argon atmosphere.

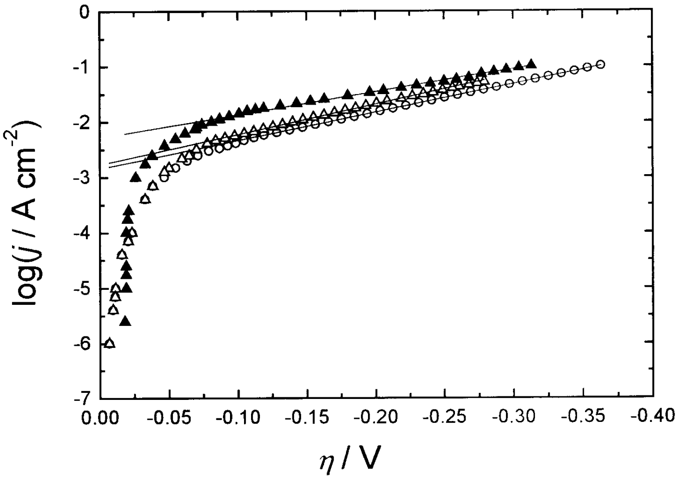

Figure 6. The steady-state polarization curves for the HER in 5 *M* KOH at 25°C on the Ni-P + TiO_2 electrode directly after deposition (o) and after heating in argon at 400°C (Δ) and at 500°C (▲). Continuous lines are linear approximations of the Tafel curves.

Table 1. Kinetic parameters obtained from the steady-state polarization curves for the HER in 5 *M* KOH at 25℃ on the Ni-P + TiO_2 layer before (A) and after heating in argon at 400℃ (B), and at 500°C (C).

Electrode	b (V dec^{-1})	j_0 (A cm^{-2})	η_{100} (V)
Ni-P + TiO_2 (A) Ref. 10	–0.197	$(1.43\pm0.04)\times10^{-3}$	–0.363
Ni-P + TiO_2 heated at 400°C (B)	–0.187	$(1.74\pm0.05)\times10^{-3}$	–0.279
Ni-P + TiO_2 heated at 500°C (C)	–0.259	$(5.98\pm0.18)\times10^{-3}$	–0.312

The apparent exchange current density determined for electrode A ($j_0 = 1.43\cdot10^{-3}$ A cm^{-2}, $\eta_{100} = -363$ mV) is close to that obtained for electrode B ($j_0 = 1.74\cdot10^{-3}$ and $\eta_{100} = -279$ mV) and lower than for electrode C ($j_0 = 5.98\cdot10^{-3}$ A$\cdot$cm^{-2} and $\eta_{100} = -312$ mV). Obviously, the heating of Ni-P + TiO_2 electrode leads to the increase in the exchange current density and in apparent activity towards HER (characterized by η_{100}) comparing to electrode A.

Considering a decrease in the surface area of the heated Ni-P + TiO_2 electrodes (see Figs. 1–4 and Tab. 1), the increase in their electrochemical activity is probably connected with the increase of their intrinsic (real) activity. This is in a good agreement with our earlier results concerning Ni-P + titanium oxides electrodes. The presence of numerous active centres enhances the activity of the heated coatings towards HER more than the large surface development [7,11,16].

Ac impedance spectroscopy. In order to study the electrode activity, *ac* impedance technique was applied. In Figure 7 typical complex plane plots obtained for Ni-P + TiO_2 electrodes before and after heating at 400 and 500℃ are shown. The measurements were performed in 5 *M* KOH, at 25°C.

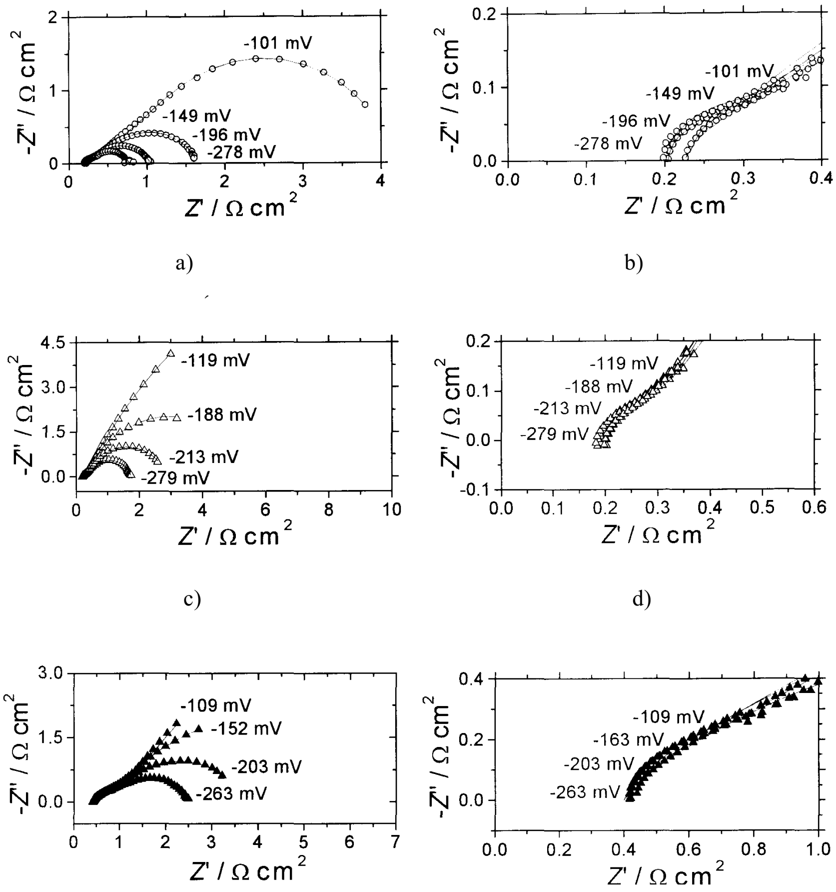

a) b) c) d) e) f)

Figure 7. Experimental complex-plane plots obtained on the Ni-P + TiO_2 electrode before (a) and after heating in argon at 400°C (c) and at 500°C (e) for the HER in 5 *M* KOH at 25°C at various overpotentials in the whole range of frequencies, and at high frequencies range (b, d, f). The continuous lines indicate the fitted data using CNLS method.

Complex plane plots (Fig. 7a–f) usually serve for selecting the equivalent circuits [2,5,6]. One major disadvantage of these plots is that there is no direct dependence of the impedance on the frequency of the applied signal. Since Bode plots provide such information, they were used to display EIS data (Fig. 8a–c). Phase angle Bode plots are especially sensitive to the modelling errors. Approximations of Nyquist and Bode plots are very good (Figs. 7, 8).

Two semicircles in Nyquist plots were obtained for unheated Ni-P + TiO_2 electrode (A) within the entire potential range (Fig. 7a). Complex plane plots obtained for the heated electrodes (B, C) exhibit porous behaviour (Fig. 7c–f). The first semicircle of the constant radius is almost potential-independent, while the second one decreases with the increase of η and its radius equals to the charge transfer resistance, R_{ct}. These results are consistent with those obtained on porous electrodes. For such

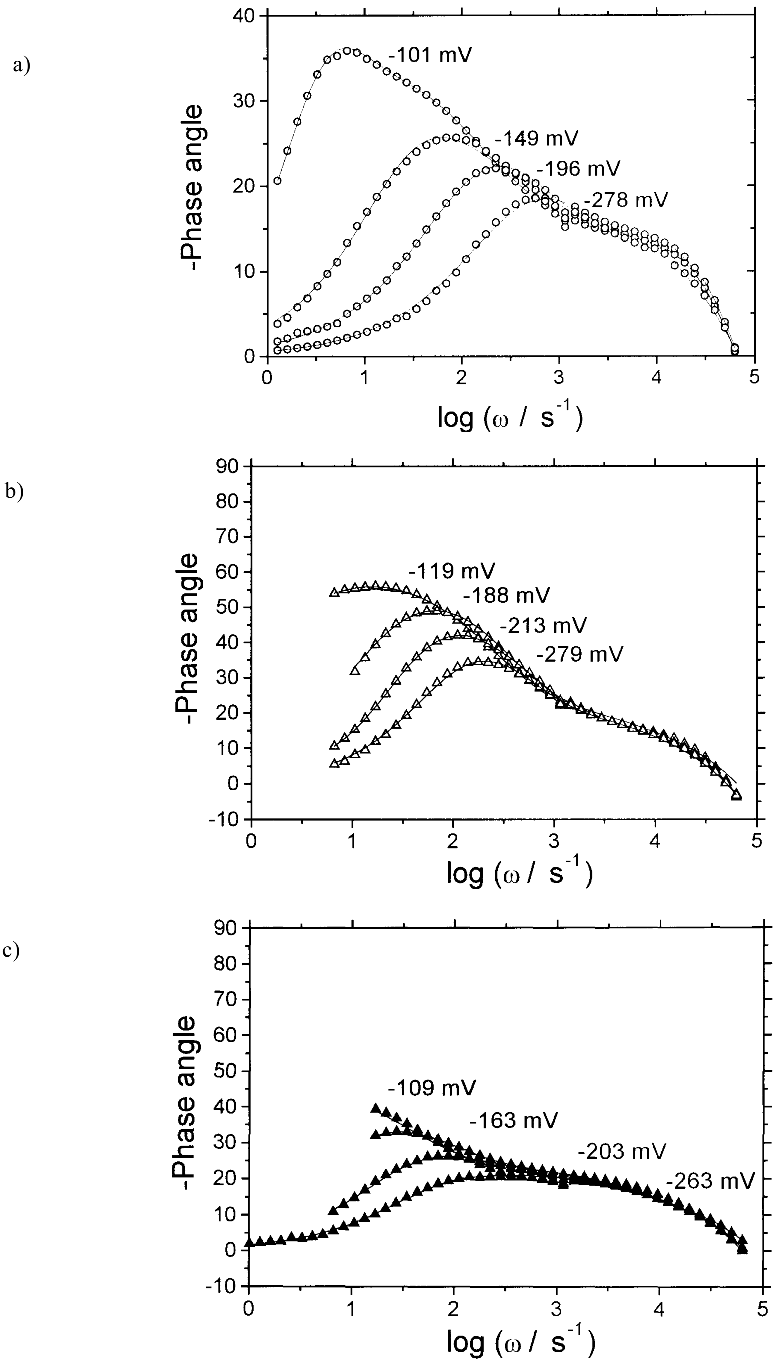

Figure 8. Phase-angle Bode plots obtained for the HER in 5 *M* KOH at 25°C on the Ni-P + TiO_2 electrode before (o) and after heating in argon at 400°C (Δ), and at 500°C (▲) for the HER in 5 *M* KOH at 25°C at various overpotentials. Points are experimental data, continuous lines are CNLS approximation.

electrodes, the high-frequency part of the complex plane plots is either a straight line of a slope of 45°, or a semicircle for cylindrical and pear-shaped pores, respectively [2,5–7]. According to the complex non-linear least squares (CNLS) approximations [2,5,6–11,21,22,25,25,26,30–33], the impedance of electrode A may be replaced with the following circuit: solution resistance, R_S connected in series with the parallel connection of R_1-CPE$_1$ (related to the porosity), and with another R_{ct}-CPE parallel circuit. CPE denotes the double layer capacitance of the impedance given by $Z_{CPE} = 1/T\,(j\omega)^{\phi}$ [29], where ϕ stands for a dimensionless parameter related to the constant phase angle, $\alpha = 90°\,(1-\phi)$ [25], and T is a capacity parameter related to the average double layer capacitance, C_{dl}: $T = \overline{C}_{dl}^{\phi}\left(R_s^{-1} + A\right)^{1-\phi}$ [29]. R_S is the solution resistance and $A = 1/R_{ct}$.

Experimental impedance values obtained at electrodes B and C may be accurately approximated by the porous model. This model provides one with such quantities as the solution resistance, R_S, charge transfer resistance, R_{ct}, solution resistance within pores, $R_{\Omega,p}$, and the parameters characterizing double layer. An inductance, L, is added in series with the solution resistance. This simple porous electrode model was described earlier [26]. The presence of L is important at high frequencies, especially for large currents and low impedance [27,28].

The results of the CNLS approximations as a function of the overpotential, η, *i. e.* log R_{ct}, C_{dl} and ϕ, are shown in Figure 9.

R_{ct} values (Fig. 9a) determined for all electrodes are a decreasing function of the potential. Charge-transfer resistance values for HER are similar in the whole range of overpotentials, except from the lowest η. R_{ct} values for the heated electrodes are slightly smaller than those determined for the unheated electrode. This is indicative for some changes in the electrochemical behaviour of the heated electrodes compared to electrode A. The presence of TiO_2 and the increased amount of non-stoichiometric Ti oxides might be responsible for synergetic effects on HER.

For electrodes B and C, the electrolyte resistance within the pore axis, $R_{\Omega,p}$, [26] was also determined. This parameter depends on the geometry of the pore and on the solution resistance ($R_S = 0.149\ \Omega\ cm^2$), however should be independent on the potential. $R_{\Omega,p}$ values were constant in the applied overpotential range, and are equal to 0.519 ± 0.01 and $2.219 \pm 0.01\ \Omega\,cm^2$ for electrode B and C, respectively. The validity of the porous electrode model involving inductance, $L = (3.4 \pm 0.084) \times 10^{-6}$ H and $(7.04 \pm 0.022) \times 10^{-6}$ H for electrode B and C, respectively, has been confirmed.

Differential double-layer capacities for Ni-P + TiO_2 electrodes were estimated using the equation proposed by Brug *et al.* [29], and successfully applied in our earlier papers to Ni-based electrodes [7,9–11,16,21,26,30–33]. C_{dl} values for electrode A depend linearly on overpotential [10], (Fig. 9b). They decrease from 40 ± 5 mF cm^{-2} at less negative η to 3.0 ± 0.3 mF cm^{-2} at more negative overpotentials. This may suggest that the real surface area available for HER decreases with an increase of η. A decrease of the electrochemically acitive surface area of Ni-P + TiO_2 electrode with an increase of overpotential is due to the blocking of pores by the released bubbles of gaseous hydrogen. When the electrode overpotential increases, intensive evolution

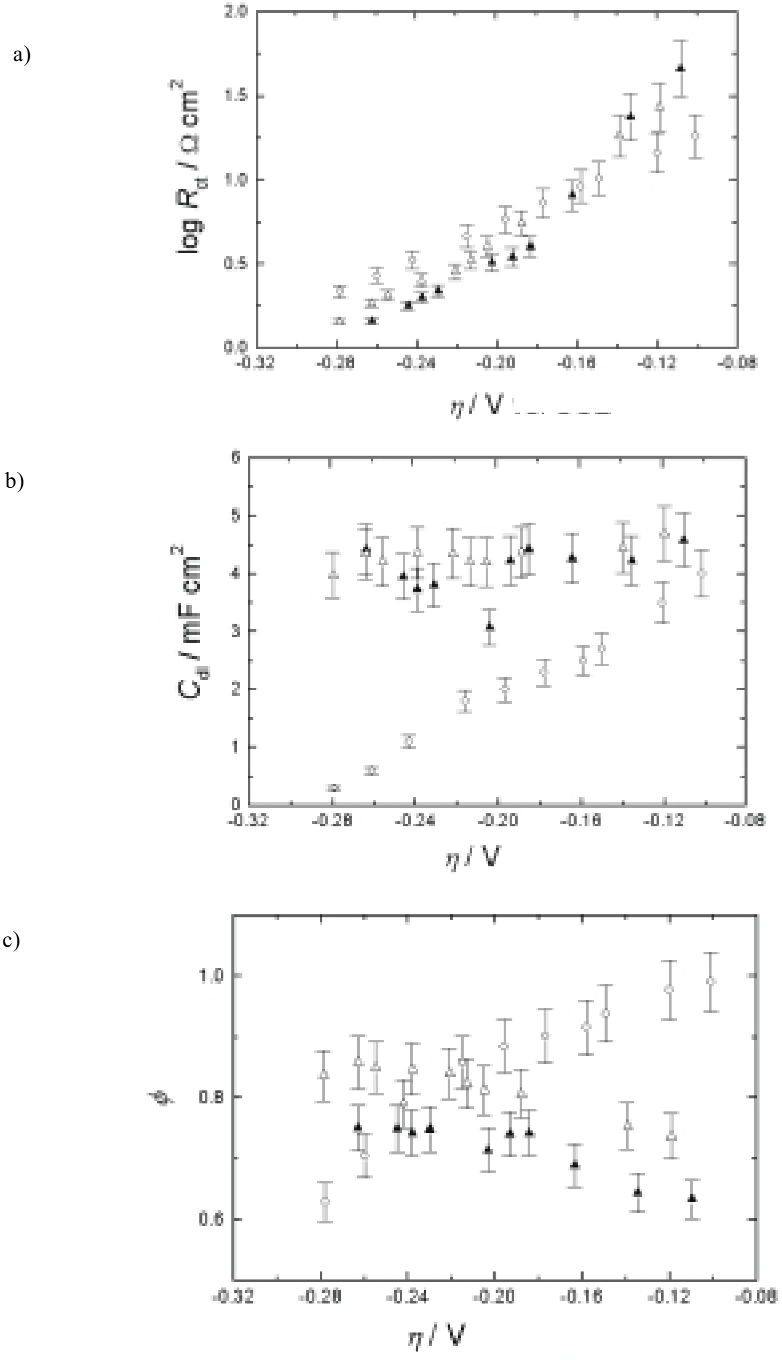

Figure 9. Dependence of logarithm of the charge-transfer resistance, R_{ct}, (a), double-layer capacitance, C_{dl}, (b) and constant phase angle, ϕ, parameter of the CPE (c) on overpotential, η, for the HER in 5 *M* KOH at 25°C on the Ni-P + TiO_2 electrode before (o) and after heating in argon at 400°C (Δ), and at 500°C (▲).

of small hydrogen bubbles is observed, which can be strongly inhibited inside the pores present on the surface of the electrode. The phenomenon of blocking of the electrode surface is more pronounced compared to the situation at low overpotentials [7].

C_{dl} values for the heated electrodes are comparable with those obtained for electrode A at low η, and remain constant with the overpotential. They are equal to 43 ± 4 and 41 ± 4 mF cm^{-2} for electrode B and C, respectively. Thus, the electroactive surface area of the heated electrodes is constant, contrary to what was found for electrode A. From GSS results and our earlier AES results for Ni-P + TiO_2 electrode surface, the presence of TiO_2 and Ti_2O_3 [10,13] was confirmed. The increased amount of Ti_2O_3 was responsible for the improved activity of the heated electrodes.

Figure 9c shows the overpotential dependence of parameter ϕ of the CPE element for electrode A. The ϕ value decreases from approximately 0.99 ± 0.007 at low overpotentials to 0.63 ± 0.049 at high η. Therefore, the increase of overpotential is followed by a strong change of the surface roughness. ϕ parameter characterising the electrode surface inhomogeneity, remains approximately constant for the electrodes heated at 400 and 500°C: 0.817 ± 0.004 and 0.72 ± 0.02, respectively. However, parameter ϕ strongly deviates from unity due to the surface structure of composite Ni-P + TiO_2 coatings. According to the literature [25,34,35], this phenomenon may be also caused by the adsorption of ions.

In Fig. 10 the logarithm of the inverse charge-transfer resistance, A, ($A = 1/R_{ct}$) is plotted *vs.* overpotential. For electrode A, the linear dependence of the slope close to that of Tafel plot (see Tab. 1) is observed. At the potentials larger than 180 mV (Fig. 6), the slopes (dE/dlog R_{ct}) for both heated electrodes are smaller compared to the Tafel slope (164 and 176 mV dec^{-1} for electrode B and C, respectively). Using the non-lin-

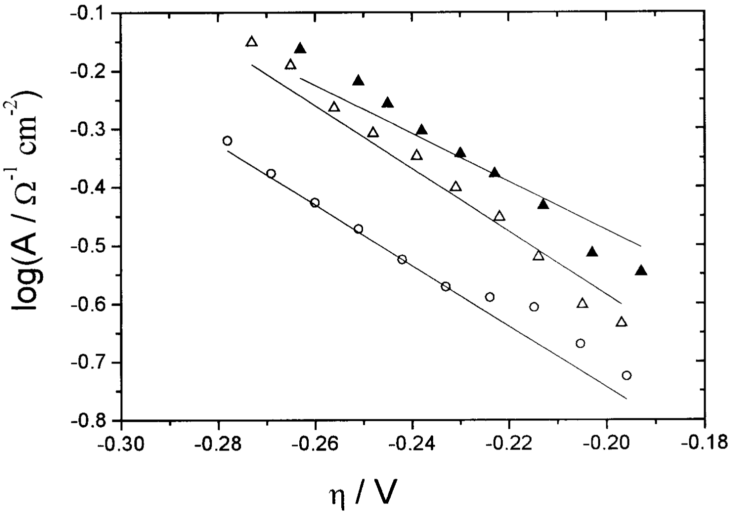

Figure 10. Dependence of the logarithm of the inverse charge-transfer resistance, $A = 1/R_{ct}$, on overpotential, η, for the HER in 5 M KOH at 25°C on the Ni-P + TiO_2 electrode before (o) and after heating in argon at 400°C (Δ), and at 500°C (▲). Straight lines are linear approximations of the experimental curves.

ear least squares (NLS) fitting, A values from EIS studies and j values from the steady-state measurements were plotted against η. The approximation involved the adjustment of the rate constants and the charge-transfer coefficient. This procedure was described earlier in [2,5,6–11,21,22,30–33].

Assuming the two-step Volmer-Heyrovský reaction mechanism of HER, the experimental results were approximated – solid lines on Figures 6 and 10. The corresponding kinetic parameters and their standard deviations are given in Table 2.

Table 2. Comparison at $\eta = -100$ mV of the apparent and the real kinetic parameters of the HER obtained from steady-state and *ac* impedance experiments in 5 *M* KOH on the Ni-P + TiO_2 electrode before and after heat-treatment.

Electrode	k_{av} (mol cm^{-2} s^{-1})	$\alpha_1 = \alpha_2$	R_f	j_0/R_f (A cm^{-2})	$k_{intrinsic} = k_{av}/R_f$ (mol cm^{-2} s^{-1})
Ni-P + TiO_2 (A) Ref. 10	$(7.03\pm0.12)\times10^{-9}$	0.309 ± 0.002	2000 ± 100	7.15×10^{-7}	3.50×10^{-12}
Ni-P + TiO_2 heated at 400°C (B)	$(8.87\pm0.35)\times10^{-9}$	0.321 ± 0.004	2201 ± 110	7.90×10^{-7}	4.03×10^{-12}
Ni-P + TiO_2 heated at 500°C (C)	$(2.65\pm0.14)\times10^{-8}$	0.246 ± 0.005	2110 ± 110	2.84×10^{-6}	1.26×10^{-11}

For the electrodes examined at 25°C in 5 *M* KOH, transfer coefficients of the Volmer-Heyrovský reactions, α_1 and α_2 ($\alpha_1 = \alpha_2$) were determined (Tab. 2). It is known that there are two equivalent sets of parameters, which describe the Volmer-Heyrovský mechanism, since permutation of charge-transfer coefficients and rate constants does not affect experimental results ($\alpha_1 \Leftrightarrow \alpha_2$, $k_1 \Leftrightarrow k_2$, $k_{-1} \Leftrightarrow k_{-2}$) [36,37]. At more negative potentials the values of parameters k_{-1} and k_{-2} were negligibly small and did not need to be determined. In such a case, an average rate constant, k_{av}, ($1/k_{av} = 1/k_1 + 1/k_2$) was obtained [7,10,11] and the approximation of Tafel plots and EIS data for the examined electrodes was possible (Tab. 2). The rate constant, k_{av}, increases with an increase of the heating temperature. For electrode C, k_{av} is one order of magnitude larger compared to the value obtained for electrode A (with respect to the geometric surface areas of the electrodes). Transfer coefficient is also smaller for A, which indicates the change in the mechanism and lowers the apparent electrode activity. For electrode C the transfer coefficient is twice as high, which is typical for $\alpha = 0.5$ and consistent with the porous model [5,38].

Assuming the average capacitance of a smooth metal surface C_{dl} to be 20μF cm^{-2} [39], the surface roughness, R_f, was estimated (Tab. 2). The ratios of the double layer capacitances of the examined and smooth metallic electrodes are potential-dependent only in the case of electrode *A*. R_f values for electrode A estimated at (–100 mV) and average R_f values for electrodes B and C are given in Table 2. Obviously, the heating influences R_f of Ni-P + TiO_2 electrode only slightly. The roughness factor increases from 2000 ± 100 for A to 2201 ± 110 for B, and 2110 ± 110 for C electrodes. Therefore, the ratio of the electrochemically accessible (true) to the geometric surface areas characterised by R_f is similar for all the electrodes. The results of GSS analysis point at a slight decrease of the surface area after heating. However, these measurements do not allow one to detect micropores on the surface, while from the *ac* impedance results one can determine the total surface area being in contact with the solution.

The intrinsic activity of the electrodes may be evaluated from the apparent exchange current densities, j_0, and kinetic parameters, k_{av}, divided by the estimated roughness factor [2,5,6–11,21,22,30–32]. The apparent values, as well as the determined ones (per unit of the real surface area) are listed in Table 2. The highest intrinsic activity for HER is observed at 25°C in 5 *M* KOH at electrode C ($j_0/R_f = 2.84 \times 10^{-6}$ A cm^{-2}, $k_{intrinsic} = 1.26 \times 10^{-11}$ mol cm^{-2} s^{-1}). The intrinsic activity, k_{av}/R_f of that electrode is one order of magnitude higher than that of A and B electrodes. The comparison of k_{av} values is presented in Table 2. According to these results, the apparent activity of electrode A ($k_{av} = 7 \times 10^{-9}$ mol cm^{-2} s^{-1}) is close to that of electrode B, but one order of magnitude smaller as compared to that of electrode C ($k_{av} = 2.6 \times 10^{-8}$ mol cm^{-2} s^{-1}). The 3.7-fold increase of the apparent rate constant, k_{av}, (Table 2) originates from the increase in the intrinsic activity, $k_{intr}(C)/k_{intr}(A) \cong 3.6$. The obtained values are consistent with those found for composite Ni-P + TiO_2 + Ti and Ni-P + TiO_2 + Ti_7O_{13} coatings [7,10,11,16].

Noteworthy, the observed increase in the intrinsic rate constant is partially compensated by the increase in the transfer coefficient, which, in turn, leads to the moderate decrease of parameter η_{100}. Having in mind a decreased electrochemical activity of the heated Ni-P electrodes [2,5–7,10–13,25] towards HER, one can attribute the synergetic effect in the case of the heated Ni-P + TiO_2 electrodes towards hydrogen reduction/adsorption on TiO_2 and Ti_2O_3 surface. It should be noted that this assumption is valid for Ni-P coatings containing more than 12 at.% of phosphorous. In the case of unheated Ni-P + TiO_2 electrode, nanosize crystallites of the amorphous Ni-P matrix hinder the access to Ti_2O_3 + TiO_2 phases during HER more than after heating. After the heat treatment, the coatings with considerably larger crystallites of nickel and nickel phosphides are formed. This change in the surface structure is so significant, that electrochemical access to Ti_2O_3 species is improved. Under such conditions, Ti_2O_3 and TiO_2 phases reveal a synergetic effect, despite the presence of nickel and nickel phosphides in the heated coatings. As a result, kinetic parameters of HER on such electrodes are improved. This effect is accompanied by insignificant increase of R_f, which is proportional to the electrochemically active surface area. However, the increased content of Ti_2O_3 is undetectable with XRD.

The Volmer-Herovský mechanism of HER at the examined electrodes should include the participation of non-stoichiometric titanium oxides, and is similar to that reported in the earlier paper [10,11]. Most probably, the presence of titanium oxides facilitates decomposition of water and induces electrochemical surface reactions accompanying HER in the alkaline solution. After the heating of Ni-P + TiO_2 coatings, the enhancement of HER results probably from the increased quantity of non-stoichiometric titanium oxides.

CONCLUSIONS

Electrolytically deposited composite coatings consist of an amorphous nickel-phosphorus matrix, in which crystalline micro-particles of TiO_2 (anatase) are embedded. The heating of composite Ni-P + TiO_2 electrocoatings in the argon atmosphere facilitates the transformation of Ni-P matrix to Ni and Ni_5P_2 phases, while TiO_2 (anatase) remains unchanged. The surface roughness of deposits apparently decreases with the increase of the heating temperature.

Ac behaviour of Ni-P + TiO_2 electrodes before and after heating can be successfully explained using the porous model. It has been shown that at any of the examined electrodes in 5 *M* KOH and at 25°C, HER proceeds *via* the Volmer-Heyrovský mechanism with the participation of titanium oxides. It has been found that electrode activity towards HER increases after heating, due to the increased amount of non-stoichiometric Ti oxides, compared to the unheated Ni-P + TiO_2 electrode (Ti oxides influence surface reduction/adsorption of hydrogen). The electrodes examined are potentially applicable to the alkaline electrolysis of water.

The list of symbols

A	Inverse of charge-transfer resistance, Ω^{-1} cm^{-2}
Ar	Relative real surface area of the coating, %
b	Slope of the Tafel plot, V dec^{-1}
C_{dl}	Differential double-layer capacitance, F cm^{-2}
f	Frequency of potential sinusoidal perturbation, Hz
j	Total current assuming the Volmer-Heyrovský reaction mechanism for the HER, A cm^{-2}
j_0	Apparent exchange current density, A cm^{-2}
k_{av}	Average rate constant, mol cm^{-2} s^{-1}
k_i	Rate constant of the forward reaction step (i), mol cm^{-2} s^{-1}
k_{-i}	Rate constant of the backward reaction step (i), mol cm^{-2} s^{-1}
k_{intr}	Intrinsic rate constant of step (i), mol cm^{-2} s^{-1}
L	Inductance, H
l	Sampling length, mm
R_a	Arithmetical mean deviation of the roughness profile, μm
R_{ct}	Charge-transfer resistance, Ω cm^2
R_f	Roughness factor
R_p	Maximum roughness profile peak height, μm
R_S	Solution resistance, Ω cm^2
R_v	Maximum roughness profile valley depth, μm
R_z	Ten point height of irregularities, μm
$R_{\Omega,p}$	Electrolyte resistance within the pore axis, Ω cm^2
RL_0	Developed roughness profile length, mm
RL_n	Evaluated roughness profile length, mm
RS	Average distance between irregularities, μm
T	Capacity parameter, F cm^{-2} s$^{\phi-1}$
Z	Impedance, Ω cm^2
Z_f	Faradaic impedance, Ω cm^2
Z'	Real component of impedance, Ω cm^2
Z''	Imaginary component of impedance, Ω cm^2

Greek letters

α_i	Symmetry coefficient related to step (i)
ϕ	CPE exponent
Θ	Surface coverage by adsorbed hydrogen
η	Hydrogen overpotential, V

η_{100}	Hydrogen overpotential at current density of 100 mA cm^{-2}, V
ω	Angular frequency

Abbraviations

AES	Auger electron spectroscopy
CPE	Constant-phase element
CNLS	Complex non-linear least squares fitting program
EDTA	Ethylenediaminetetraacetic acid
EIS	Electrochemical impedance spectroscopy
FRA	Frequency response analyser
GSS	Geometric surface structure
HER	Hydrogen evolution reaction
NLS	Nonlinear least squares fitting program
SEM	Scanning electron microscope
XRD	X-ray diffraction
2D	Two-dimensional
3D	Three-dimensional

Acknowledgments

Scientific support of Professor J. Cybo and his assistance with the Form Talysurf surface analyser is gratefully acknowledged.

REFERENCES

1. Breiter M., Handbook of Fuel Cells – Fundamentals, Technology and Applications, Edited by W. Vielstich, H.A. Gasteiger, A. Lamm, vol. 2: Reaction mechanisms of the H_2 oxidation/evolution reaction, John Wiley & Sons, Chichester 2003.
2. Lasia A., Handbook of Fuel Cells – Fundamentals, Technology and Applications, Edited by W. Vielstich, H.A. Gasteiger, A. Lamm, vol. 2: Electrocatalysis – Hydrogen Evolution Reaction, John Wiley & Sons, Chichester 2003, pp. 416–440.
3. Trasatti S., Advances in Electrochemical Science and Engineering, H. Gerischer and C.W. Tobias (Eds), VCH, Weinheim, vol. 2, 1992, p. 2.
4. Wendt H. (Ed), Electrochemical Hydrogen Technologies, Elsevier, Amsterdam, 1990.
5. Lasia A., Modern Aspects of Electrochemistry (edited by B.E. Conway and R.E. White), vol. 35, Kluwer Academic/Plenum Publishers, New York 2002, p. 1.
6. Lasia A., Modern Aspects of Electrochemistry (edited by B.E. Conway, J. Bockris and R.E. White), vol. 32, Kluwer Academic/Plenum Publishers, New York 1999, p. 143.
7. Łosiewicz B., Doctoral Thesis, Institute of Physics and Chemistry of Metals, University of Silesia, Katowice 2002.
8. Erler F., Jakob C., Romanus H., Spiess L., Wielage B., Lampke T. and Steinhäuser S., *Electrochim. Acta*, **48**, 3063 (2003).
9. Panek J., Serek A., Budniok A., Rówiński E. and Łągiewka E., *Int. J. Hydrogen Energy*, **28,** 169 (2003).
10. Łosiewicz B., Budniok A., Rówiński E., Łągiewka E. and Lasia A., *Int. J. Hydrogen Energy*, **29**, 145 (2004).
11. Łosiewicz B., Budniok A., Rówiński E., Łągiewka E. and Lasia A., *J. Appl. Electrochem.*, **34**, 507 (2004).
12. Gruszka A. and Budniok A., *Adv. Perform. Mater.*, **6**, 141 (1999).
13. Gierlotka D., Rówiński E., Budniok A. and Łągiewka E., *J. Appl. Electrochem.*, **27**, 1 (1997).
14. Łosiewicz B., Stępień A., Gierlotka D. and Budniok A., *Thin Sol. Films*, **349**, 43 (1999).
15. Napłoszek-Bilnik I. and Budniok A., *Kompozyty* (*Composites*), **2**, 63 (2002).
16. Łosiewicz B., Budniok A., Lasia A., Rówiński E. and Łągiewka E., Proceedings of The 203rd Meeting of The Electrochemical Society, Abstract No 2684, Le Palais des Congres, Paris, April 27–May 2, 2003, France.

17. Napłoszek-Bilnik I., Budniok A., Łosiewicz B., Pająk L. and Łągiewka E., *Thin Sol. Films* (to be published).
18. Lasia A., *J. Electroanal. Chem*., **397**, 27 (1995).
19. Cybo J., Gołąb A. and Służałek G., Solidification of Metals and Alloys, PAN, Katowice, vol. 2, 2000, p. 432–438.
20. ISO 468-1982, Surface roughness – Parameters, their values and general rules for specifying requirements.
21. Hitz C. and Lasia A., *J. Electroanal. Chem*., **500**, 213 (2001).
22. Hitz C. and Lasia A., *J. Electroanal. Chem*., **532**, 133 (2002).
23. Brown A.P., Krumpelt M., Loutfy R.O. and Yao N.P., *J. Electrochem. Soc.,* **129**, 2481 (1982).
24. Brown A.P., Krumpelt M., Loutfy R.O. and Yao N.P., *Electrochim. Acta,* **27**, 557 (1982).
25. Karimi Shervedani R. and Lasia A., *J. Electrochem. Soc*., **144**, 511 (1997).
26. Valøen L.O., Lasia A., Jensen J.O. and Tunold R., *Electrochim. Acta*, **47**, 2871 (2002).
27. Göhr H., Mirnik M. and Shiller C.A., *J. Electroanal. Chem*., **180**, 273 (1984).
28. Karunathilaka S.A.G.R., Barton R., Hughes M. and Hampson N.A., *J. Appl. Electrochem*., **15,** 251 (1985).
29. Brug G.J., van den Eeden A.L.G., Sluyters-Rehabach M. and Sluyters J.H., *J. Electroanal. Chem*., **176**, 275 (1984).
30. Karimi Shervedani R. and Lasia A., *J. Appl. Electrochem*., **29**, 979 (1999).
31. Karimi Shervedani R. and Lasia A., *J. Electrochem. Soc*., **145**, 2219 (1998).
32. Chen L. and Lasia A., *J. Electrochem. Soc*., **140**, 2464 (1993).
33. Lasia A., *Curr. Topics Electrochem*., **2**, 239 (1993).
34. Pajkossy T., *J. Electroanal. Chem*., **364**, 11 (1994).
35. Dumont H., Los P., Brossard L., Lasia A. and Ménard H., *J. Electrochem. Soc*., **139**, 2143 (1992).
36. Lasia A. and Rami A., *J. Electroanal. Chem.*, **294**, 123 (1990).
37. Gennero de Chialvo M.R. and Chialvo A.C., *J. Electrochem. Soc*., **147**, 1619 (2000).
38. de Levie R., Advances in Electrochemistry and Electrochemical Engineering, P. Delahay, Ed., vol. 6, Interscience, New York, 1967, p. 329.
39. Trasatti S. and Petrii O.A., *Pure Appl. Chem*., **63**, 711 (1991).